Frontiers of Information Technology & Electronic Engineering
www.jzus.zju.edu.cn; engineering.cae.cn; www.springerlink.com
ISSN 2095-9184 (print); ISSN 2095-9230 (online)
E-mail: jzus@zju.edu.cn

Simultaneous wireless information and power transmission system based on a dual-frequency metasurface design

Yicen LI, Mingyang CHANG, Hao XUE, Haixia LIU, Long LI[†‡]

School of Electronic Engineering, Xidian University, Xi'an 710071, China

[†]E-mail: lilong@mail.xidian.edu.cn

Received Apr. 30, 2024; Revision accepted Oct. 4, 2024; Crosschecked

Abstract: Nowadays, the number of wireless sensor devices is increasing rapidly, posing persistent challenges related to battery replacement and power wiring. This paper presents a simultaneous wireless information and power transmission (SWIPT) scheme based on a frequency diversity metasurface design, which provides a wireless power supply scheme for electrical devices such as sensors. The metasurface is designed with frequency bands commonly found in the environment, and achieves efficient absorption of electromagnetic (EM) energy at 5.8 GHz and radiation of sensor information at 2.45 GHz, making it possible to take full advantage of the energy in the environment and easy to integrate with existing systems. The branches for the dual-square-loop are designed based on spatial impedance matching and equivalent circuit, giving the metasurface advantages such as compact size (unit size of 0.16 ×0.16 ×0.012 λ_0, where λ_0 is the wavelength at 2.45 GHz), high isolation (S_{21}<-20 dB within the operating frequency band), and insensitivity to incident angles (maintaining over 80% efficiency within 60° angles). Integrated with rectification circuits and sensors, it efficiently converts EM waves received by the metasurface into DC power for sensor operation. The sensors then radiate information through the metasurface, effectively addressing challenges related to sensor device wiring and battery replacement, thereby offering new solutions for the development of next-generation smart cities.

Key words: Frequency diversity; Metasurface design; Simultaneous wireless information and power transmission (SWIPT); Sensor

https://doi.org/10.1631/FITEE.2400345 **CLC number:**

unedited

1 Introduction

Since the start of the 21st century, wireless communication technology (WIT) and the Internet of Things (IoT) have experienced rapid development, leading to the continuous expansion of wireless communication. This growth has been accompanied by a geometric increase in electronic devices, particularly in the case of implantable medical devices for humans and tens of thousands of miniaturized, low-power wireless sensors (Shibata et al., 2001; Cheng et al., 2013; Bakogianni and Koulouridis, 2016; Li et al., 2018). However, there are still some challenges such as wiring difficulties and the high cost of battery replacement in these devices (Xue et al., 2024). The emergence of simultaneous wireless information and power transmission (SWIPT) technology allows for energy provision to communication devices while exchanging information, thereby overcoming the limitations of traditional batteries and wired connections. It provides a new approach to supplying power for sensors, enabling electronic devices to break free

‡ Corresponding author

* Project supported by the National Key Research and Development Program of China under Grant 2023YFB3811503, National Natural Science Foundation of China under Grant 62288101, the Key Research and Development Program of Shaanxi under Grant 2021TD-07, and by the Fundamental Research Funds for the Central Universities (20103224952)

ORCID: Yicen LI, https://orcid.org/00009-0004-5263-0845; Mingyang CHANG, https://orcid.org/0000-0002-2790-4638; Hao XUE, https://orcid.org/0009-0001-6234-7208; Haixia Liu, https://orcid. org/ 0000-0003-2610-5751; Long LI, https://orcid.org/0000-0003-0472-7314

© Zhejiang University Press 2024

from the constraints of batteries and power lines, thereby extending their lifespan (Piñuela et al., 2013; Andrews et al., 2014; Fang et al., 2015; Wang X et al., 2023; Liu et al., 2024).

In SWIPT systems, the current mainstream methods include frequency diversity and polarization diversity. For frequency diversity, a dual-channel frequency-reconfigurable antenna for the SWIPT system was designed (Lu et al., 2017). A planar dipole antenna was used as the receiving antenna and introduced defect ground structures were introduced to enhance isolation between the two ports, achieving efficient SWIPT for different scenarios. A dual-band wearable antenna were designed using conductive textiles (Wagih et al., 2021). Coupled feeding was used a square patch to generate resonance at 2.4 GHz with a gain of 7.2 dBi for WiFi communication, while the planar dipole was successfully miniaturized through bending and integration with the patch, achieving resonance for energy harvesting in the lower frequency band (785-875 MHz). For polarization diversity, a dual-polarization rectenna antenna for the SWIPT system was proposed (Yang et al., 2013). By using slot-coupled feeding, the patch antenna achieved dual polarization at 5.8 GHz frequency, with high isolation between ports, using the characteristics of polarization diversity to achieve synergistic energy and information transmission. A two-orthogonally-polarized Huygens line antenna was designed to form a dual-polarization antenna (Lin and Ziolkowski, 2019). Similarly leveraging polarization diversity, they achieved energy-harvesting communication in the 915 MHz ISM frequency band and realized antenna miniaturization and high port isolation of 30 dB through a tightly coupled feeding design.

The SWIPT system has grown by leaps and bounds in recent years, due to the subwavelength unit cells of metasurfaces. These typically exhibit compact, miniaturized, and rotationally symmetrical structural characteristics, and have advantages such as polarization insensitivity and wide-angle incidence. Consequently, significant research effort is being applied to metasurfaces for the design of radio frequency (RF) energy harvesting devices (Zhong et al., 2016; Zhang et al., 2017; El Badawe et al., 2018; Yu et al., 2018; Erkmen et al., 2021; Wang CC et al., 2022). A compact and polarization-insensitive rectenna based on a metasurface was designed at a frequency of 5.8 GHz (Chang et al., 2024). A multi-frequency and multi-mode metasurface was also designed for efficient RF and microwave energy harvesting (Huang et al., 2023). A novel rectifying metasurface with high efficiency was designed for use in low power scenarios (Lee and Hong, 2020). A polarization-independent dual-band metasurface absorber based on an improved Minkowski fractal structure was proposed for wireless power transmission (Gao et al., 2023).

These designs achieve efficient absorption of electromagnetic (EM) energy, but require miniaturization and high port isolation to reduce interference with information during energy transmission which is applied in the SWIPT system. Traditional rectifier antennas often require a complex feeding network to achieve dual polarization or high port isolation. This complexity not only increases energy loss but also enlarges the array during design. To address these challenges, we present a dual-frequency metasurface designed for SWIPT systems (Fig. 1). The proposed system uses the approach of frequency diversity to enable efficient energy harvesting and transmission within a more compact form, that uses two commonly used frequency bands, 5.8 GHz for RF-DC conversion and 2.45 GHz for sensor data transmission. The metasurface structure is engineered to absorb electromagnetic energy efficiently, ensuring high port isolation in a smaller size. Additionally, integrated sensors enable the self-powering of small appliances, effectively eliminating the need for regular battery replacement.

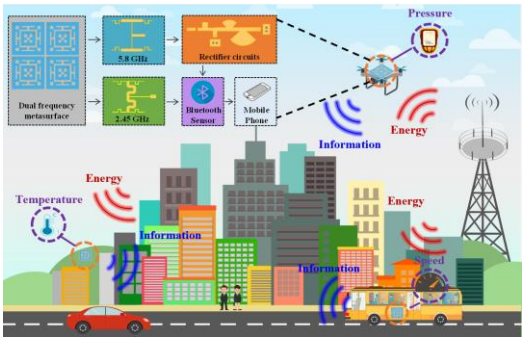

Fig. 1 System operation principle diagram

2 Theory and methods

Here, we present the theory and methods for the producing high-performance dual-frequency metasurface.

unedited

2.1 Design of the metasurface unit

The design process of the unit is shown in Fig. 2. The unit of the metasurface consists of a radiating and receiving common-aperture structure on the surface, an S7136H dielectric substrate (dielectric constant=3.55, loss tangent=0.0039) in the middle, and a metal ground at the bottom.

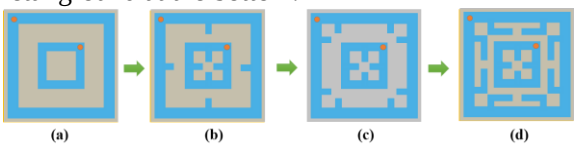

Fig. 2 The process of unit design

To realize the metasurface achieving dual-frequency in a smaller size, the design process of the structure of the unit was as follows: firstly, we use a dual-square-loop design to realize the two frequencies: the outer loop working at low frequency, and the inner loop working at high frequency (Fig. 2a). Secondly, to achieve miniaturization, branches are added to the dual-square-loop to extend the current path (Fig. 2b). However, due to the limited spacing between the dual-square-loops, it is not feasible to add long branches to the inner loop for miniaturization. The two branches are added to the outer loop to further achieve miniaturization at low frequency because of the longer wavelength of 2.45 GHz compared with 5.8 GHz (Fig. 2c). Finally, the length of the two branches is extended to work at 2.45 GHz (Fig. 2d).

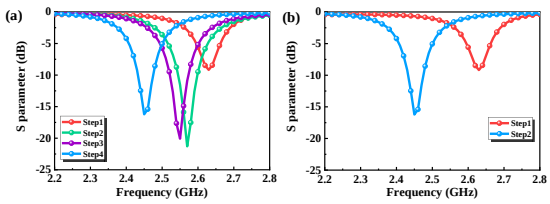

Fig. 3 The effect of the unit structure on parameters (a), the outer loop (b), the inner loop

Simulations were conducted using ANSYS software to observe the impact of the design process on the unit frequency (Fig. 3). The designed unit was placed in an air box with a periodic boundary, along with Floquet ports to simulate the performance parameters of the unit. The two Floquet ports at the top and bottom were designated port f1 and port f2, respectively, while the feeding ports on the unit were designated port 1 and port 2. For the lower frequency, the unit showed a simulated S_{11} of -9.18 dB at 2.63 GHz in the step1, -21.28 dB at 2.57 GHz in the step2, -20.07 dB at 2.55GHz in step3 and -16.21 dB at 2.45 GHz in step4. For the higher frequency, the unit has a simulated S_{11} of -13.33 dB at 6.1 GHz in step1 and -18.98 dB at 5.7 GHz in step2. The current path increases with the increase of the branches, the frequency shifts to lower, and finally the two required operating bands are realized.

Compared with a rectified antenna, the design of the metasurface needs to consider not only the impedance matching of the loads but also the matching of the intrinsic impedance Z of the metasurface with the free space Z_0 when performing energy reception. Therefore, the structure of the metasurface can be adjusted to improve the efficiency of energy reception. The intrinsic impedance of the metasurface can be denoted (Fante and McCormack, 1988):

$$Z=\sqrt{\frac{\mu}{\varepsilon}}=\sqrt{\frac{\mu_0}{\varepsilon_0}}\sqrt{\frac{\mu_r}{\varepsilon_r}}=Z_0\sqrt{\frac{\mu_r}{\varepsilon_r}} \qquad (1)$$

where $\mu_0=4\pi\times10^{-7}$ H/m represents the vacuum permeability, $\varepsilon_0=8.854\times10^{-12}$ F/m represents the vacuum dielectric constant, μ_r and ε_r represent the relative permeability and relative permittivity of the metasurface respectively, and $Z_0=120\pi$ represents the intrinsic impedance of free space. When the EM wave is incident on the metasurface, the reflection coefficient Γ can be expressed as:

$$\Gamma=\frac{Z-Z_0}{Z+Z_0}=\frac{\sqrt{\mu_r/\varepsilon_r}-1}{\sqrt{\mu_r/\varepsilon_r}+1} \qquad (2)$$

If we want higher absorption efficiency, Γ has to be close to zero, which means the relative permeability of the metasurface is equal to its relative permittivity, $\mu_r=\mu_r'-j\mu_r''=\varepsilon_r'-j\varepsilon_r''$.

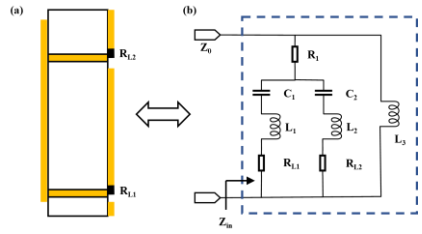

Fig. 4 (a) The side view of the unit, and (b) the equivalent circuit of the unit

The equivalent circuit was used to analyze the influence of the dual-square-loop structure on absorption efficiency (Fig. 4). R_{L1} and R_{L2} represent the

Unedited

terminal load, R_1 represents the metal and medium loss, L_3 represents the inductance between the metal of the top and bottom layers, and the inner and outer loops can be equivalent to a separate LC resonant circuit, which are parallel. (Langley and Parker, 1983) has already provided a detailed derivation of relevant parameters. Therefore, according to the equivalent circuit, the impedance of the unit can be expressed as:

$$Z_1 = \frac{1}{j\omega C_1} + j\omega L_1 + R_{L1} \tag{3}$$

$$Z_2 = \frac{1}{j\omega C_2} + j\omega L_2 + R_{L2} \tag{4}$$

$$Z = (R_1 + Z_1 \square Z_2) \square (j\omega L_3) \tag{5}$$

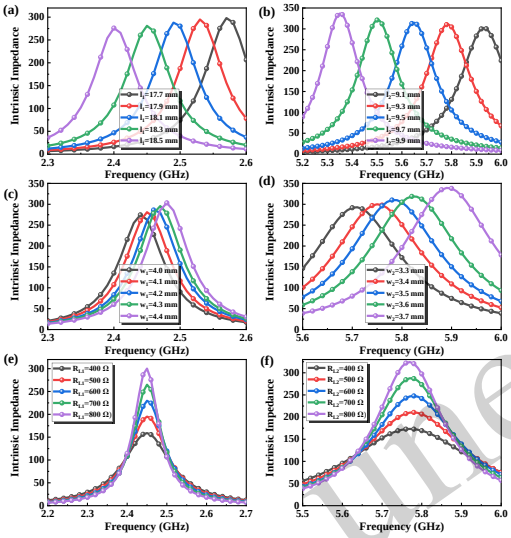

Fig. 5 The effect of the unit (a) l_1 at 2.45 GHz, (b) l_2 at 2.45 GHz, (c) w_1 at 5.8 GHz, (d) w_2 at 5.8 GHz, (e) R_{L1} at 2.45 GHz, (f) R_{L2} at 5.8 GHz on intrinsic impedance

Based on the above analysis, there are two ways of adjusting the efficiency of EM absorption:1). Adjusting the structure of the unit to affect the equivalent capacitive inductance value, using adjusted unit impedance for matching with the spatial impedance (Fig. 5a, b, c, d; 2). Adjusting the terminal load to match the unit impedance with the spatial impedance (Fig. 5e, f). Note that because the unit structure is equivalent to LC resonant circuits, not only will the impedance be adjusted, but the resonant frequency also changes while adjusting the unit structure.

The effect of the branches on the unit was analyzed (Fig. 6). By decreasing s and increasing l_3, the lower frequency of the unit can be effectively shifted lower (Fig. 6a, b). By increasing the length and width of the inner branches, the higher frequency of the unit can be effectively shifted lower (Fig. 6c, d). Note that due to the introduction of the branches, the impedance of the unit will also be affected. Therefore, we can flexibly adjust the relevant parameters of the branches on the inner and outer loop to realize the requirements for the frequency of the unit.

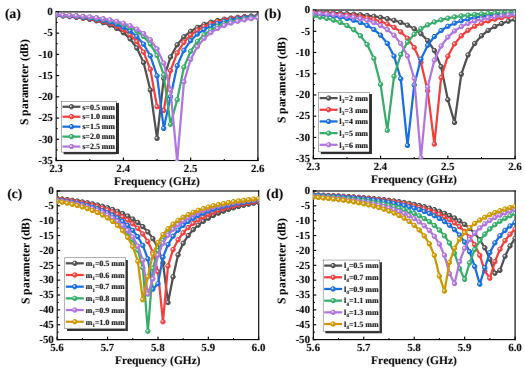

Fig. 6 Parameter scan of inner and outer branches (a), the impact of 's' at 2.45 GHz (b), the impact of 'l_3' at 2.45 GHz (c), the impact of 'm_1' at 5.8 GHz (d), the impact of 'l_4' at 5.8 GHz

After completing the above analysis of the unit structure, we were satisfied that the unit met the requirements. Its structure is shown in Fig 7. The relevant parameters are as follows: p=20 mm, l1=18 mm, l2=9.3 mm, l3=8.4 mm, l4=2 mm, s=0.9mm, m1=0.9 mm, h=1.524 mm. The top common aperture structure adopts a dual-square-loop with branches suitable for two frequency bands. The unit cell size p=20 mm is smaller than half a wavelength, which effectively addresses the issue of half-wavelength spacing between elements in traditional antennas. The impedance at both feeding ports is set to 750 Ω for loads matching. The feeding ports are located at the two diagonals of the loops, with port 1 placed at the outer ring for information transmission and port 2 placed at the inner ring for energy transmission. The radius of the metalized via holes is 0.25 mm. The calculation of energy harvesting efficiency, taking port 1 as an example, is as follows:

$$A = \frac{P_L}{P_t} = 1 - \left|S_{f_1 f_1}\right|^2 \tag{6}$$

where P_L represents the amount of energy received by the load, and P_t represents the total transmitted power. Therefore, the energy received at port 1 of the unit, is the total transmitted energy minus the energy returned to the transmitting port.

Unedited

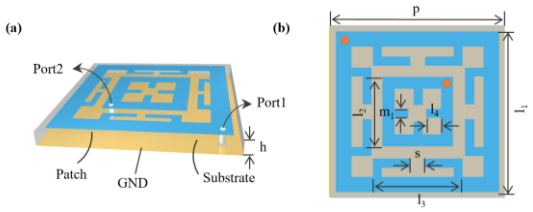

Fig. 7 Layout of the metasurface (a), stereo view (b), top view

The performance of the unit was analyzed (Fig. 8). Ports 1 and 2 had reflection coefficients below -10 dB within the frequency bands of 2.41-2.49 GHz and 5.71-5.85 GHz, reaching below -25 dB at 2.45 GHz and 5.8 GHz.

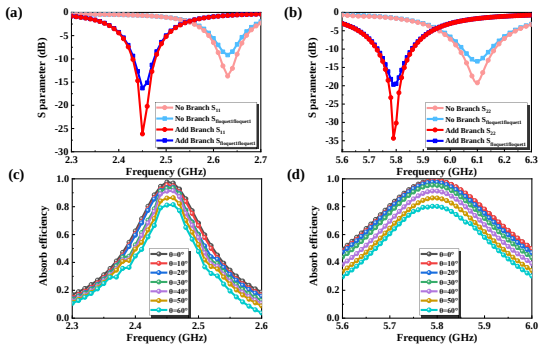

Fig. 8 Reflection coefficient with/without branch and absorption efficiency at different angles of incidence (a), reflection coefficient at 2.45 GHz (b), reflection coefficient at 5.8 GHz (c), absorption efficiency at 2.45 GHz (d), absorption efficiency at 5.8 GHz

Through the above analysis, the energy harvesting efficiency calculated by Eq. 6 yields the efficiency. The unit showed high energy harvesting efficiency in both frequency bands. To validate the unit's wide-angle energy harvesting characteristics, the elevation angle of the incident wave was varied, and the energy harvesting efficiency changed with the incident angle (Fig. 8c, d). With increasing elevation angle, there was a slight frequency offset in the peak efficiency, and the peak efficiency also decreased. However, within a 60° angle, the energy harvesting efficiency at 2.45 GHz and 5.8 GHz remained above 80% which shows that the designed unit structure has the ability to collect EM energy from space at wide angles.

To better understand the operation of the two frequencies of the unit, we analyzed the electric field distribution of the dual-square-loop in different bands obtained under incident wave absorption (Fig. 9). The outer loop and the added outer branches were involved mainly at 2.45 GHz and the inner loop and the added inner branches played a major role at 5.8 GHz, showing that the added branches can effectively achieve miniaturization. The dual-square-loops had little effcet on each other in the two working bands, which verifies the high isolation of the unit.

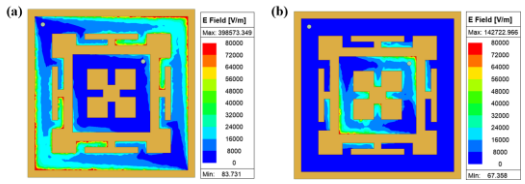

Fig. 9 The electric field distribution of the unit at (a), 2.45 GHz (b), 5.8 GHz

2.2 Design of the metasurface array

In this section, we describe a 2×2 array we designed to validate the performance (Fig. 10). A layer of dielectric substrate was added below the metasurface, and two 4-to-1 power combiners were used to combine the four ports at 5.8 GHz and 2.45 GHz into one port each. To facilitate the lamination of the two layers of dielectric substrates and the integration of rectifier circuits, the array was expanded from 40×40 mm to 50×50 mm. The dielectric substrate for the power combiners used S7136H, with a thickness of 0.762 mm.

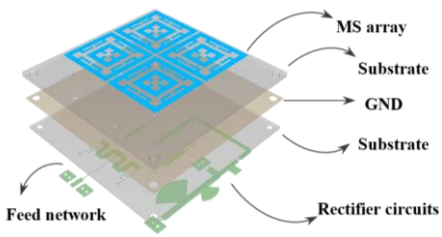

Fig. 10 An exploded diagram of the metasurface array

The simulation results shown in Fig. 11 show that the array shows good consistency with the resonance characteristics of the unit. The S_{11} at 2.45 GHz and 5.8 GHz are both less than -20 dB. Additionally, the two ports show good isolation characteristics, with S_{21} values less than -20 dB in both operating frequency bands. This ensures minimal interference with information transmission while energy transfer is being conducted. The gain of the metasurface array were measured to be 4.4 dBi at 2.45 GHz and 8.98 dBi at 5.8 GHz, which were lower than the simulated values. The difference between simulation parameters

unedited

and experimental parameters was caused by machining errors, but the array still met the design requirements.

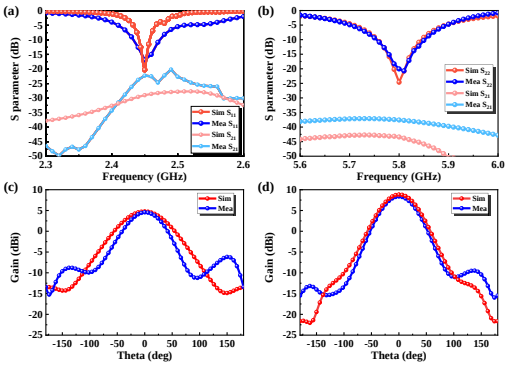

Fig. 11 Reflection coefficients and radiation pattern of the metasurface array (a), reflection coefficients at 2.45 GHz (b), reflection coefficients at 5.8 GHz (c), radiation pattern at 2.45 GHz (d), radiation pattern at 5.8 GHz

To achieve the conversion of RF energy to direct current (DC) energy, we designed a rectifier circuit integrated with the metasurface to convert the RF energy absorption at the 5.8 GHz frequency band into DC energy to directly power the sensors. The structure is shown in Fig. 12a.

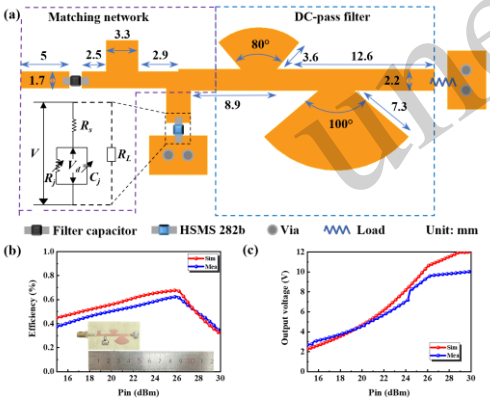

Fig. 12 The structure of the rectifier and relevant results (a), the structure of the rectifier (b), the simulation and experimental parameters of efficiency (c), the simulation and experimental parameters of output voltage

To successfully power more sensors, we chose the HSMS282b rectifier diode because of the advantage of adapting a large input power (generally the input power is greater than 20 dBm). Simulations were conducted using Advanced Design System 2020 (ADS). The slight difference between experimental and simulation was due to machining errors. Fig. 12b shows the curve of rectification efficiency versus input power obtained through joint simulation at a frequency of 5.8 GHz with a load resistance of 200 Ω. The rectification efficiency remains above 40% for input powers ranging from 12.8 to 28.8 dBm. At 26 dBm, the rectification efficiency reaches its peak value of 67.8%, indicating the high efficiency of the rectifier circuit. Fig. 12c shows the output voltage of the rectifier. The output voltage reaches 10 V when the input power reaches 25.5 dBm, which can achieve the working voltage of most sensors.

2.3 The SWIPT system based on the dual-frequency metasurface

To ensure the proposed metasurface could work successfully in the SWIPT system, we verified that the EM energy received by the metasurface can satisfy the normal operation of the sensor (Fig. 13a). Considering the space loss, we generated RF energy through the signal generator (AV1141B) and then connected it to the amplifier and radiated EM waves through the horn. The same horn was placed at a distance of 0.5 m and the power received at this time was measured. We adjusted the transmit power until the receiving horn was measured to receive 26 dBm of power. We replaced the receiving horn with the metasurface in the same position, and measured the output power at this time (Fig. 13b). The efficiency was lower than that obtained by simulation calculation because the impedance matching between the metasurface 5.8 GHz port and the input port of the rectifier circuit was poor due to errors in the actual machining process, so the overall efficiency was low, but it still realized the power demand of the sensor.

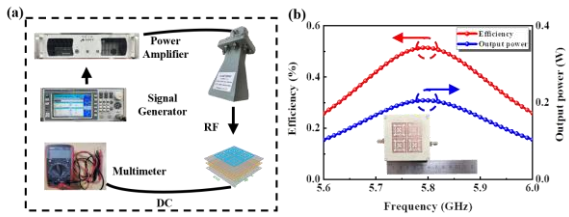

Fig. 13 Measurement of energy reception performance of the metasurface (a), a schematic view of the experiment (b), the efficiency and output power of the metasurface

To further validate the feasibility of the system, we conducted tests using a height sensor (SPL06) and a Bluetooth module (Fig. 14). The output positive and negative poles of the rectifier circuit were connected to a voltage regulator module to stabilize the output voltage at 3.3 V, which then powered the Bluetooth

unedited

module and the height sensor. After the height sensor was powered on and functioning normally, it transmited data to the Bluetooth module. The Bluetooth module was connected to the metasurface's 2.45 GHz port, and the height information was then transmitted from the metasurface. Finally, the mobile phone received the height information.

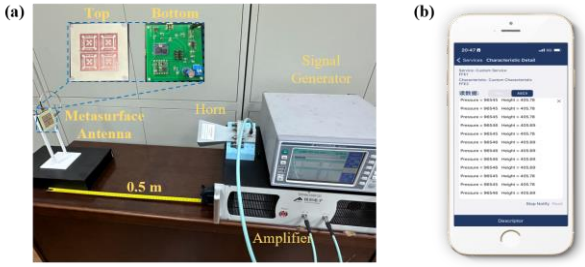

Fig. 14 (a), The measurement of the system (b), the information received by mobile phone

When the transmitting horn radiates EM waves, the metasurface receives RF energy in the 5.8 GHz frequency band. The rectifier circuit converts RF into DC energy, which then powers the sensors. After the sensors operate normally, they transmit information through the 2.45 GHz frequency band. Finally, the mobile phone receives the information sent by the sensors. This system eliminates the need for complex wiring arrangements at the back end and eliminates the need for regular battery replacements. Therefore, there is a heavy demand for the power dissipation of the electric appliance in this study because of the gas pressure sensor (10 dBm) and the Bluetooth (9 dBm), and the rectification circuit is designed with the input power considered to be large (26 dBm). The power dissipation of the sensor is low under normal conditions, and there is no need for such a large input power dissipation demand. Metasurfaces are currently being widely applied in new scenarios such as holographic MIMO (Gong et al., 2024) and SWIPT. Our design has the potential for further expansion in the future, such as using polarization diversity in the SWIPT system to effectively address the looming issue of electromagnetic resource scarcity. Additionally, more diversified chip integration can facilitate environmental sensing and adaptive transmission. These advancements offer new approaches for the construction of future smart cities.

3 Conclusions

In this paper, we present a receiving metasurface designed for the SWIPT system, which uses frequency diversity to achieve the reception of EM energy and the transmission of sensor information. The metasurface achieves efficient absorption of EM energy at 5.8 GHz and radiates sensor information at 2.45 GHz. It offers advantages such as miniaturization (unit size 0.16×0.16×0.012 λ_0), high isolation (S_{21}<-20 dB within the operating frequency band), and insensitivity to incident angles (maintaining efficiency above 80% for angles within 60°). This design provides a new solution for addressing the power supply issues of multiple sensors in future digital urban development processes.

Unedited

Contributors

Yicen LI designed the research. Yicen LI and Mingyang CHANG processed the data. Yicen LI drafted the manuscript. Haixia LIU and Hao XUE helped organize the manuscript. Hao XUE and Long LI revised and finalized the paper.

Conflict of interest

All the authors declare that they have no conflict of interest.

References

Andrews JG, Buzzi S, Choi W, et al., 2014. What will 5G be? *IEEE J Select Areas Commun*, 32(6):1065-1082. https://doi.org/10.1109/JSAC.2014.2328098

Bakogianni S, Koulouridis S, 2016. Design of a novel miniature implantable rectenna for in-body medical devices power support. Proc 10th European Conf on Antennas and Propagation, p.1-5. https://doi.org/10.1109/EuCAP.2016.7481970

Chang MY, Li YC, Han JQ, et al., 2024. A compact polarization insensitive rectenna with harmonic suppression for wireless power transfer. *IEEE Antennas Wirel Propag Lett*, 23(1):119-123. https://doi.org/10.1109/LAWP.2023.3319317

Cheng HW, Yu TC, Luo CH, 2013. Direct current driving impedance matching method for rectenna using medical implant communication service band for wireless battery charging. *IET Microwaves, Antennas Propag*, 7(4):277-282. https://doi.org/10.1049/iet-map.2012.0372

El Badawe M, Ramahi OM, 2018. Efficient metasurface rectenna for electromagnetic wireless power transfer and energy harvesting. *Prog Electromagn Res*, 161:35-40. https://doi.org/10.2528/PIER18011003

Erkmen F, Ramahi OM, 2021. A scalable, dual-polarized absorber surface for electromagnetic energy harvesting

and wireless power transfer. *IEEE Trans Microwave Theory Techn*, 69(9):4021-4028. https://doi.org/10.1109/TMTT.2021.3087622

Fang C, Yu FR, Huang T, et al., 2015. A survey of green information-centric networking: research issues and challenges. *IEEE Commun Surv Tut*, 17(3):1455-1472. https://doi.org/10.1109/COMST.2015.2394307

Fante RL, McCormack MT, 1988. Reflection properties of the Salisbury screen. *IEEE Trans Antennas Propagat*, 36(10):1443-1454. https://doi.org/10.1109/8.8632

Gao X, Wang XR, Wang WJ, 2023. Polarization-independent dual-band metasurface absorber for wireless power transmission. *J Phys*: *Conf Ser*, 2469:012003. https://doi.org/10.1088/1742-6596/2469/1/012003

Gong TR, Gavriilidis P, Ji R, et al., 2024. Holographic MIMO communications: theoretical foundations, enabling technologies, and future directions. *IEEE Commun Surv Tut*, 26(1):196-257. https://doi.org/10.1109/COMST.2023.3309529

Huang XJ, Wang K, Sun CZ, et al., 2023. A multi-frequency and multi-mode metasurface energy harvester for RF energy harvesting. *Smart Mater Struct*, 32(10):105010. https://doi.org/10.1088/1361-665X/acf424

Langley RJ, Parker EA, 1983. Double-square frequency-selective surfaces and their equivalent circuit. *Electron Lett*, 19(17):675-677. https://doi.org/10.1049/el:19830460

Lee K, Hong S K, 2020. Rectifying metasurface with high efficiency at low power for 2.45 GHz band. *IEEE Antennas Wirel Propag Lett*, 19(12):2216-2220. https://doi.org/10.1109/LAWP.2020.3027833

Li L, Liu HX, Zhang HY, et al., 2018. Efficient wireless power transfer system integrating with metasurface for biological applications. *IEEE Trans Ind Electron*, 65(4):3230-3239. https://doi.org/10.1109/TIE.2017.2756580

Lin W, Ziolkowski RW, 2019. Electrically small Huygens antenna-based fully-integrated wireless power transfer and communication system. *IEEE Access*, 7:39762-39769. https://doi.org/10.1109/ACCESS.2019.2903545

Liu HX, Li YC, Cheng FJ, et al., 2024. Holographic tensor metasurface for simultaneous wireless powers and information transmissions using polarization diversity. *Adv Funct Mater*, 34(2):2307806. https://doi.org/10.1002/adfm.202307806

Lu P, Yang XS, Wang BZ, 2017. A two-channel frequency reconfigurable rectenna for microwave power transmission and data communication. *IEEE Trans Antennas Propagat*, 65(12):6976-6985. https://doi.org/10.1109/TAP.2017.2766450

Piñuela M, Mitcheson PD, Lucyszyn S, 2013. Ambient RF energy harvesting in urban and semi-urban environments. *IEEE Trans Microwave Theory Techn*, 61(7):2715-2726. https://doi.org/10.1109/TMTT.2013.2262687

Shibata T, Sasaya T, Kawahara N, 2001. Development of in‐pipe microrobot using microwave energy transmission. *Electron Commun Jpn* (*Part II*: *Electron*), 84(11):1-8. https://doi.org/10.1002/ecjb.1067

Wagih M, Hilton GS, Weddell AS, et al., 2021. Dual-band dual-mode textile antenna/rectenna for simultaneous wireless information and power transfer (SWIPT). *IEEE Trans Antennas Propagat*, 69(10):6322-6332. https://doi.org/10.1109/TAP.2021.3070230

Wang CC, Zhang JL, Bai SB, et al., 2022. A harmonic suppression energy collection metasurface insensitive to load and input power for microwave power transmission. *IEEE Trans Microwave Theory Techn*, 70(8):4036-4044. https://doi.org/10.1109/TMTT.2022.3182238

Wang X, Han JQ, Li GX, et al., 2023. High-performance cost efficient simultaneous wireless information and power transfers deploying jointly modulated amplifying programmable metasurface. *Nat Commun*, 14(1):6002. https://doi.org/10.1038/s41467-023-41763-z

Xue H, Lu ZQ, Ma XJ, et al., 2024. A reconfigurable metasurface enhancing signal coverage for wireless communication using reduced numbers of p-i-n diodes. *IEEE Trans Microwave Theory Techn*, 72(3):1964-1978. https://doi.org/10.1109/TMTT.2023.3311952

Yang XX, Jiang C, Elsherbeni AZ, et al., 2013. A novel compact printed rectenna for data communication systems. *IEEE Trans Antennas Propagat*, 61(5):2532-2539. https://doi.org/10.1109/TAP.2013.2244550

Yu F, Yang XX, Zhong HT, et al., 2018. Polarization-insensitive wide-angle-reception metasurface with simplified structure for harvesting electromagnetic energy. *Appl Phys Lett*, 113(12):123903. https://doi.org/10.1063/1.5046927

Zhang XM, Liu HX, Li L, 2017. Tri-band miniaturized wide-angle and polarization-insensitive metasurface for ambient energy harvesting. *Appl Phys Lett*, 111(7):071902. https://doi.org/10.1063/1.4999327

Zhong HT, Yang XX, Tan C, et al., 2016. Triple-band polarization-insensitive and wide-angle metamaterial array for electromagnetic energy harvesting. *Appl Phys Lett*, 109(25):253904. https://doi.org/10.1063/1.4973282

unedited